LC-DET-2001-023
DESY
February 2001

A CCD-based Vertex Detector for TESLA

C J S Damerell
Rutherford Appleton Laboratory, Chilton, Didcot, OX11 0QX, UK
for the LCFI Collaboration
(Bristol University, Brunel University, Glasgow University, Lancaster University, Liverpool University, Oxford University, Rutherford Appleton Laboratory)

Abstract

TESLA will provide a major challenge and opportunity for flavour identification. The small-radius beam-pipe and advances in detector technology will yield unprecedented performance for *b*- and charm-tagging, as well as more sophisticated tools such as the separate identification of quark and anti-quark jets for both *b* and charm. There are several technologies which may deliver the required performance, which comprises a combination of very small pixels (for clean 2-track resolution in the core of jets), excellent mechanical stability ($< 5\,\mu$m overall measurement precision) and thin layers for acceptable multiple scattering of low momentum tracks (preferably $< 0.1\%\ X_0$). The CCD technology, building on the 307 Mpixel SLD vertex detector, offers one promising approach. This paper outlines the conceptual design of such a detector, and the R&D programme which needs to be carried out over the next few years in order to establish the feasibility of this technology to achieve the design goals set by the physics requirements. If these can be realised, TESLA will be assured of a vertex detector able to play its part as a tool for new physics and for precision measurements in the TeV regime.

1 Introduction

LEP, SLC and the Tevatron have established the importance of vertex detectors in understanding the physics accessible at high energy colliders. At TESLA, both precision measurements and particle searches set stringent requirements on the efficiency and purity of the flavour identification of hadronic jets, since final states including short-lived *b* and *c*-quarks and τ-leptons are expected to be the main signatures. High accuracy in the reconstruction of the charged particle trajectories close to their production point must be provided by the tracking detectors, in particular by the vertex detector (VTX) located closest to the interaction point, in order to perform the reconstruction of the topology of secondary vertices in the decay chain of short-lived heavy flavour particles in a complex environment. Low efficiency would be unacceptable due to the small event samples in individual processes, and low purity would generally be unacceptable due to backgrounds.

Experience at LEP and SLD shows the way forward. Jet flavour identification can be based primarily on the topological vertex structure in the jet, since this in principle allows most *B* and *D* decay modes to be detected. By aiming for good sensitivity down to decay times short compared with the mean lifetimes, high efficiencies may be realised. Distinguishing clearly between *b* and *c* jets requires additional information. This comes from the secondary and tertiary vertex topology, the charged decay multiplicity and the vertex mass, after applying corrections for missing neutrals [1].

As well as tagging *b* and *c* jets, the vertex charge (if non-zero) can distinguish *b* from $\overline{b}$, *c* from $\overline{c}$. This requires sufficient precision to distinguish between all the decay tracks and those coming from the primary vertex. Even the case of neutral *B* decays can be handled by measuring the charge dipole between the secondary and tertiary vertices, as demonstrated in SLD.

Cases where leptons (and hence neutrinos) are absent from jets are particularly valuable for precise jet energy measurement. However, the absence of a single electron in a jet is not so easily established. Due to the prevalence of converted γs, it is important to track detected electrons inwards through the thin layers of the vertex detector to establish if they were really produced in semileptonic B or D decays. As well as providing a clean sample of jets free of missing neutrinos, this procedure in principle allows corrections to be applied to jets with charged leptons (hence also neutrinos). In these cases, the jet energy measurement may be improved substantially by extending the procedure used for the p_T-corrected mass, allowing a correction for the transverse momentum of the missing neutrino.

By careful control of backgrounds, the TESLA interaction region can be made particularly favourable for the construction of a vertex detector of unprecedented performance, well-matched to the physics goals of the TeV e^+e^- regime.

In Section 2 we discuss the physics motivation by means of a few typical examples, and in Section 3 we indicate how these lead to performance goals for the detector. In Section 4 we discuss the machine-related issues which influence the vertex detector design. Combining the performance goals with the restrictions from the machine leads to an acceptable compromise for the detector features, as discussed in Section 5. Section 6 discusses the details of the CCD option in some detail, to the extent that the design has evolved to date.

How well does a detector that can be built, accessed and serviced satisfy the physics goals? The first step in addressing this question is taken in Section 7, where the generic performance in terms of 2-track resolution and impact parameter resolution is discussed. Further work on the evaluation of this detector for physics is addressed in [2].

The current status of the R&D work of the LCFI (Linear Collider Flavour ID) collaboration [3] is discussed in Section 8, as well as an outline of the plans for the next few years.

2 Physics motivation

If electroweak symmetry breaking is realised through the Higgs mechanism, the detailed study of the production and decay properties of the Higgs boson, in particular whether it satisfies the predictions for the Standard Model Higgs or some variant of SUSY Higgs, will require the future linear collider to measure its decay branching ratios with high precision. Distinguishing between the $b\bar{b}$, $c\bar{c}$, gg, $\tau\tau$ Higgs decay channels represents a major challenge for this detector system.

High energy WW production is a sensitive process with which to probe possible anomalies in the gauge boson self-couplings. To extract the full information, it is necessary to perform a complete angular analysis of the production and decay at the parton level. The favoured procedure is to analyse events in which one W decays leptonically and the other hadronically to $c\bar{s}$. The identification of the charm jet is essential for the analysis. The sensitivity of this analysis is strongly dependent on high charm tag efficiency and purity.

Efficient tagging and angular analysis of Ws is important in various supersymmetry scenarios, such as chargino pair production with

$$\tilde{\chi}_1^{\pm} \rightarrow W^{\pm}\tilde{\chi}_1^0$$

the signal being an acoplanar W pair in 4-jet final states. Charm jet identification is again important. The scalar top (*stop*) sector may produce more complex final states where both b and charm tagging are important, such as

$$\tilde{t}_1 \rightarrow b\tilde{\chi}_1^+ \rightarrow bW^+\tilde{\chi}_1^0$$

Standard model processes such as high energy $t\bar{t}$ production provide equally challenging requirements:

$$t\bar{t} \rightarrow bW^+\bar{b}W^-$$

yields most frequently a 6-jet final state, two jets being b flavoured and frequently one or two more are charm jets.

The quantitative evaluation of the significance of flavour identification for these and many other processes requires a detailed study of the expected signals, backgrounds, angular information etc. While it is true that these studies are only now beginning, the SLD experience of the synergy between electron beam polarisation, high performance vertex detection and high performance calorimetry will clearly be extended with good effect into the TeV energy regime.

3 Performance goals

At first sight, the average impact parameter of a B decay product, approximately 300 μm (independent of boost for $\beta\gamma \gtrsim 3$) suggests that modest detector performance may suffice. However, this is misleading for several reasons. Firstly, the average impact parameters for τ and charm particle decay products are 3-4 times smaller. Equally importantly, in recent years the physics advantages have been established of detector systems which permit the correct assignment of nearly

all tracks to primary, secondary or tertiary vertices. Determination of the vertex mass and charge are examples which permit greatly improved *b/c* separation and the classification of jets as *b* or $\overline{b}$, *c* or $\overline{c}$. The importance of the vertex detector in many physics analyses which go beyond simple *b*-tagging increases at higher collider energies with more complex events, each containing a large number of jets of various flavours.

The impact parameter resolution of a detector is a convolution of the point measurement precision, lever arms, mechanical stability and multiple scattering effects. One might hope that higher energy colliders would permit a relaxation of the concerns regarding multiple scattering, but this is not the case. Even in a 1 TeV e^+e^- collider, the average energy of particles in jets (depending on the physics process) is in the region 1-2 GeV. The most interesting events will probably have high jet multiplicity, where the problems are worst. Consequently, the detector design still needs to be pushed to the limit as regards layer thickness.

Whatever performance is achieved for jets which are optimally oriented with $\theta \approx 90^o$, the impact parameter precision degrades at small polar angles due to the increased distance of the first hit from the IP, and the increased thickness of material traversed by the oblique tracks. For lower energy colliders, it was reasonable to restrict the analysis to say 90% of the solid angle. At TESLA, this will no longer be the case, firstly because an event with high jet multiplicity will have a significant probability that one of the jets is found in the extreme forward or backward region, and secondly because much of the physics relies on having spin-polarised electrons and/or positrons, where the significance of events becomes highly weighted in favour of the forward-backward direction.

Taking account of all these effects, the ideal vertex detector would consist of a series of nested low-mass spherical shells of radii *R*, 2*R*, 3*R*,.. where $R \approx 5$ mm (so as to track most of the parent *B*s and *D*s) and point-measurement precision $\sim 1\ \mu$m, with small apertures for the entry and exit beams. The separation between layers would be sufficient to control multiple scattering effects, and the number of layers would be sufficient for stand-alone track reconstruction. Reality, in the form of machine-related constraints, mechanical supports, electrical connections and cooling systems, conspires to drive the detector design away from this ideal. Fortunately, solutions can be found which largely preserve the required physics capability.

4 Machine-related issues

The luminosity and bunch timing at TESLA, combined with the requirement of untriggered operation, impose particular constraints on the vertex detector. Data need to be stored somewhere (preferably local to the detector) through the 1 ms bunch train, then transferred to the processor selected to handle the data for that bunch train. For successive trains, data are transferred to different members of the processor farm. It is not necessary for the data from the vertex detector to correlate with a unique bunch crossing. On the contrary, it is acceptable to accumulate the signals over a number of bunch crossings (as at SLD) provided that the hit density is everywhere sufficiently low that the track fitting is not significantly compromised. The CCD detector option takes advantage of this important tradeoff, which favours high granularity and moderate readout speed. The optimal solution depends on the magnitude of the machine background. In TESLA, the dominant e^+e^- pair background from the beam-beam interaction is confined radially by the 4T magnetic field of the detector solenoid. Consequently, the background is strongly peaked in layer-1, and falls rapidly beyond; thus the readout of layer-1 needs to be the fastest. Due to constraints on the design of the machine collimation system, it is necessary to set the beam-pipe radius at 14 mm. The pair background in a vertex layer just outside this beam-pipe produces about 0.03 hits/ mm^2.BX , which is acceptable for the foreseen readout system. There are 2820/4500 bunch crossings (BX) per train at 500/800 GeV, with a BX interval of 337/189 ns.

Apart from the question of hit density in the data due to the background particle flux, one has also to consider the question of radiation damage to the detector. The dominant background (pair-produced electrons which penetrate the VTX inner layer) imposes a requirement on radiation hardness of about 100 krad for a 5 year life, which is easily achieved with modern CCD technology. Potentially more serious is the neutron background. This is currently estimated to be of the order of 10^9 1 MeV-equivalent neutrons/cm^2.year, which is acceptable with current CCD designs, and there is scope for major performance improvements, which could produce a large safety factor in radiation tolerance.

5 Detector features

Since the inner layer needs to be as close as possible to the IP, the optimal design for this layer will certainly be cylindrical, just outside the beam-pipe, extending in length to cover the required polar angle range. [In the case of a linear collider, there are many reasons not to pursue the option of part or all of the vertex detector being inside the machine vacuum.] With a radius of 15 mm defined by the machine, it is has been demonstrated [4] that a pixel-based detector with pixels of size well below $50\times50\ \mu\mathrm{m}^2$ is required in order to avoid confusion (cluster merging) within the cores of high energy jets.

Beyond layer-1, there are essentially two options. For sufficiently thin detectors, the optimal arrangement is a series of cylindrical layers with the same polar angle coverage as layer-1, stepped in radius similarly to the ideal spherical system referred to in Section 3. However, if the layer thickness exceeds ~ 0.5% X_0, the penalty in material thickness at small polar angles becomes excessive, and breaking the barrel geometry with conical endcaps becomes preferable.

The CCD design, which profits from thin layers is shown in Figures 1 and 2. The inner 3 layers extend to $|\cos\theta| = 0.96$, with 5-layer coverage to $|\cos\theta| = 0.9$. The outer 4-layers are used for stand-alone track reconstruction. The advantages of stand-alone reconstruction in tracking sub-detectors are well-established; they include internal alignment optimisation, efficiency monitoring of the other tracking systems (notably the SIT/TPC) and vice versa, optimal identification of γ conversions within the vertex detector and optimal rejection of 'bad' hits due for example to cluster merging between signal and background hits.

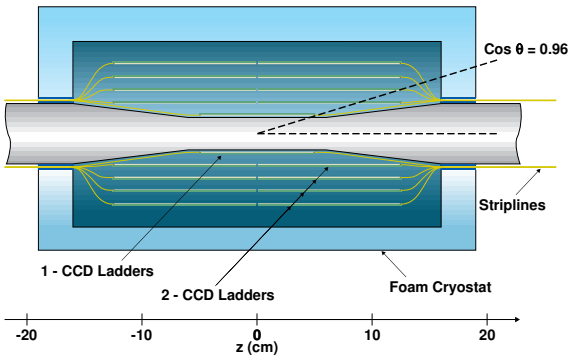

Figure 1: Cross-section of vertex detector. Cylindrical support shell linking the beam-pipe at $|z| \approx 15$ cm is not shown.

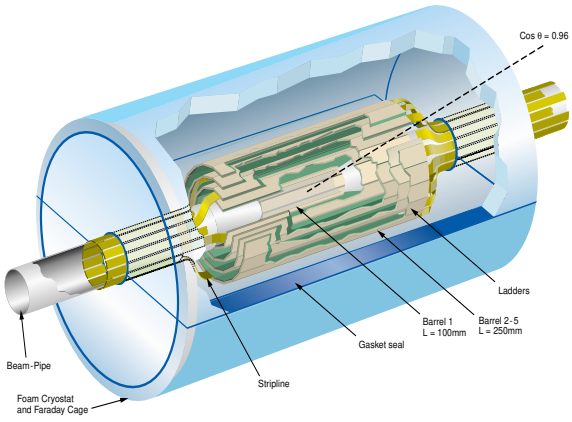

Figure 2: Isometric view of the vertex detector, again without showing the support shell

Having found the tracks in layers 2-5 (and rejected a low level of fake tracks by linking to the SIT and TPC) the layer-1 hits are used solely to refine the track extrapolation to the IP, which is particularly important for low momentum particles.

Figures 1 and 2 shows the detector inside its low-mass foam cryostat, used to permit an operating temperature of around 180 K. Not shown in the figures is the high precision mechanical support structure (a closed beryllium cylinder) which is mounted off the beam-pipe inside the cryostat. Being outside the volume used for the precision measurements and extrapolation to the IP, this cylinder can be relatively robust (approximately 2 mm wall thickness). It serves the additional role of clamping the two sections of beam-pipe rigidly together (clamps at z about ± 15 cm) so that the critical inner cylindrical section of beam-pipe of length 12 cm and radius 14 mm can be made extremely thin: 0.25 mm wall thickness beryllium is considered possible. Striplines and optical fibres are routed along the beam-pipe below the polar angle range used for tracking, connecting to inner electronics mounted in the form of a thin shell on the outer surface of the SR mask assembly.

The vertex detector will be an extremely sophisticated part of the TESLA detector. Along with other elements of the inner detector system (everything inside the TPC inner radius) it will potentially need periodic maintenance and upgrades. For this reason, there needs to be a clear plan for carrying out such operations without a major impact on other delicate equipment such as the final focus magnet system. A procedure for avoiding such interference has been devised, and is based on a strategy of rolling the TPC along the beam-line by about 5 m, to provide access to the inner detector. This follows the procedure used successfully in the SLD experiment, where access for installation of an upgrade detector was conveniently available.

6. Conceptual detector design

Unlike previous CCD-based vertex detectors, the new design will use relatively high resistivity epitaxial material, depleted all the way to the edge of the epitaxial layer. The p^+ substrate is mostly removed by mechanical lapping and chemical etching, leaving a thin residual p^+ layer. On current thinking, the epi-layer thickness will be 20-30 μm , and the overall detector thickness about 60 μm . This architecture will ensure fast collection of the min-I signal into the CCD buried channel about 1 μm below the surface.

Due to the Lorentz angle in the 4T field, the stored signal is dispersed 'horizontally' (across the CCD columns in $r\phi$ direction). Despite the 'vertical' clocking (in z direction) at 50 MHz, phasing of the clocks with the bunch crossings is expected to result in negligible vertical dispersion of the signal charge. Detailed optimisation of the pixel dimensions will depend on full 3-D simulation of the charge generation, storage and transfer to the edge of the CCD, but it is expected that optimised values (H and V) will lie in the range 20-30 μm .

As shown in Figures 1 and 2, the thin CCDs in layers 1-3 comprise all the material in the fiducial volume out to $|\cos\theta| = 0.96$, used for high precision tracking for vertex reconstruction. Beyond this volume, material is less critical and one can afford mechanical supports and readout electronics. This approach illustrates both the strengths and weaknesses of the CCD design. The advantage is unprecedented quality of impact parameter measurement, due to the minimal material and heat load, allowing the critical volume to be cooled by a gentle flow of nitrogen gas. The disadvantage is the requirement to transfer the signal charge packets out of the fiducial volume before they can be sensed. The innermost layer consists of single-CCD ladders, read out from both ends, while layers 2-5 are made of 2-CCD ladders, joined by a thin silicon bridge and read out from the outer ends only. Thus in some cases signals of about 1000 electrons have to be transferred faithfully over a distance of

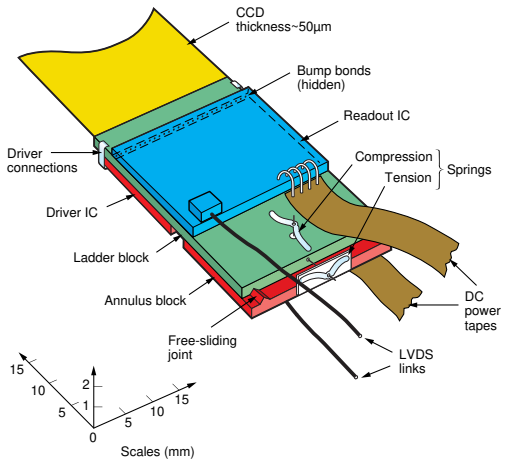

Figure 3: Layout of components at end of ladder

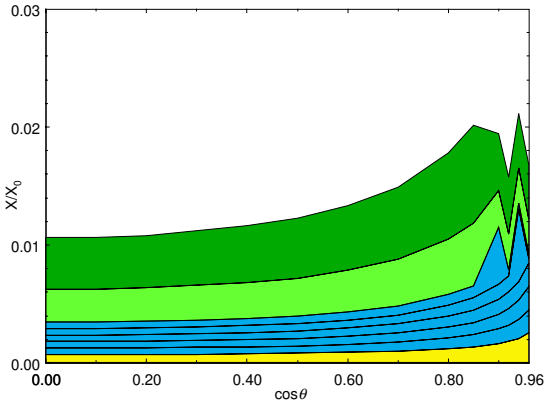

Figure 4: Material budget as function of polar angle (beam-pipe, each of 5 layers, support shell and cryostat)

up to 12.5 cm (~ 6000 pixels) en route to the CCD output. While this is a standard procedure for scientific grade devices, achieving this at high speed and in a non-negligible radiation environment is challenging. All the thin ladders are stabilised mechanically by being bonded to 'ladder blocks' which are able to slide along rigidly supported 'annulus blocks', the ladders being pinned at one end and held under tension by springs at the other (sliding) end as shown in Figure 3. This support system extends the principles pioneered in the SLD vertex detectors [5,6]. As well as providing the mechanical support for the CCD, each ladder block carries the local electronics components in the form of two or three integrated circuits. The driver chip (see Figure 3) generates the waveforms which shift the stored signals row by row down the device. The readout chip receives the analogue signals from all columns in parallel as they are shifted out of the active area to buffer amplifiers. This chip incorporates analogue-to-digital conversion, correlated double sampling to suppress reset noise in the charge-sensing circuit, data sparsification by a sequence of pixel- followed by cluster-comparators, and data storage.

Some of the key parameters associated with the detector design are listed in Table 1. The number of pixels (799×10^6 in total) assumes a pixel size of $20\times20\ \mu m^2$. Processed data stored in the readout ICs during the bunch train, amounting to ~ 8 MB, are read out via a few optical fibres between trains. The power dissipation in the drive and readout ICs will considerably exceed the capability of gas cooling. In this region, the material budget is far less critical and one can consider a more robust cooling system, specifically evaporative nitrogen cooling as used successfully in the CCD vertex detector of the CERN NA32 experiment [7], the first particle physics experiment in which a pixel-based vertex detector was used.

Layer	Radius	CCD L×W	CCD size	Ladders and CCDs/lddr	Row clock fcy and Readout time	Bgd occupancy	Integrated bgd
	mm	mm^2	Mpix			Hits/mm^2	kHits/Train
1	15	100×13	3.3	8/1	50 MHz/50 μs	4.3	761
2	26	125×22	6.9	8/2	25 MHz/250 μs	2.4	367
3	37	125×22	6.9	12/2	25 MHz/250 μs	0.6	141
4	48	125×22	6.9	16/2	25 MHz/250 μs	0.1	28
5	60	125×22	6.9	20/2	25 MHz/250 μs	0.1	28

Table 1: Key parameters of the vertex detector design. Background occupancy is based on calculated density per BX multiplied by number of BX during readout of that layer.

The material budget is shown in Figure 4. The beam-pipe and critical first 3 layers amount to 0.25% X_0 at $\cos\theta = 0$ and rise to only 0.8% X_0 at $|\cos\theta| = 0.96$. The detector has 5-hit coverage to $|\cos\theta| = 0.9$, beyond which the end supports and electronics of layers 5 and 4 are encountered. The support shell and cryostat, while contributing material at all angles, are relatively benign, being beyond the region of high precision tracking. By the time the particles encounter this material, their impact parameters are well measured.

7 Generic detector performance

In this section, we discuss simulations based on the complete TESLA tracking system, namely the vertex detector, intermediate tracking detector (ITC) and main tracking detector (TPC) operating in a 4T solenoid field. Details of these studies are reported in [2]. This work is an update of studies carried out with an earlier detector description [8].

It must be emphasised that one of the other detector technology options for the vertex detector may eventually reach or exceed these performance figures. Furthermore, CCDs might be ruled out due to unexpectedly large neutron or other hadronic backgrounds, or due to an inadequate R&D programme. There is still time for completely new ideas to emerge. For these reasons, the detector architecture to be selected remains open. However, it can be expected that the detector which is eventually installed will deliver at least the performance represented by these simulations.

One figure of merit for any pixel-based vertex detector can be expressed by the precision with which one measures the track impact parameter to the IP, separately in the $r\phi$ and rz projections. For a set of cylindrical detectors, this resolution can be expressed as

$$\sigma = \sqrt{a^2 + \left(\frac{b}{p \sin^{\frac{3}{2}} \theta} \right)^2}$$

The constant a depends on the point resolution and geometrical stability of the detectors and b represents the resolution degradation due to multiple scattering, which varies with track momentum p and polar angle θ. For the present detector design, the values of a and b are similar for both projections, and take the values 4.2 μm and 4.0 μm respectively. An example is plotted in Figure 5. These calculations are based on a full GEANT description of the TESLA detector, and use the BRAHMS detector simulation program.

The other important performance parameter is the 2-track resolution, which is particularly relevant to the core of high energy jets where the particles traverse the inner VTX layer. With a clean 2-track resolution in space of about 40 μm, CCDs are relatively robust. However, some *B*s decay close to or beyond layer 1, so there are inevitably complex examples. Experience from NA32 shows that these long-lived particles will form a particularly clean category, given unambiguous information from the outer layers. However, these questions need detailed study.

8 R&D Programme

The proposed detector with 799 Mpixels is a reasonable evolution from the successful SLD vertex detector of 307 Mpixels which operated reliably for several years in hostile background conditions. However there are challenges which push the design well beyond the performance required for SLD. R&D for the mechanical and thermal design is discussed in Section 8.1, that for the novel CCD

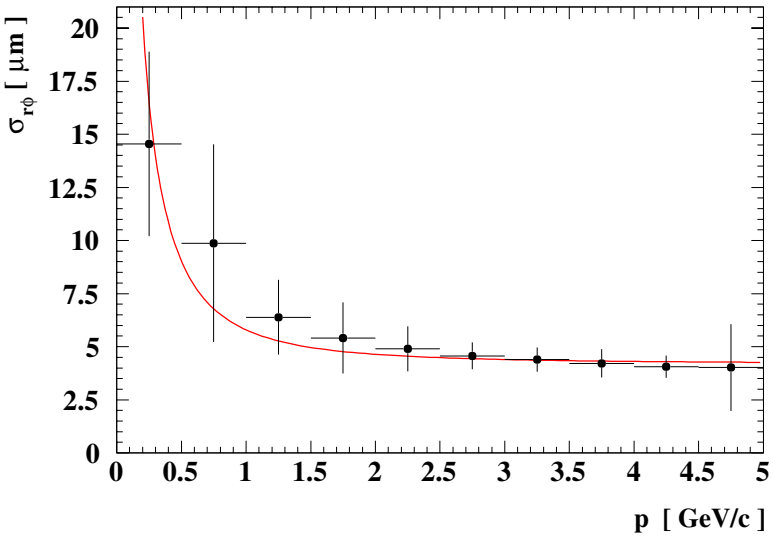

Figure 5: Track impact parameter resolution in $r\phi$ vs momentum for $\theta = 90^{o}$, for 4T solenoid field

architecture in Section 8.2, with the associated readout IC in Section 8.3, and the driver IC in Section 8.4. The issue of radiation effects is discussed briefly in Section 8.5.

8.1 Mechanical and thermal design

Given that there are many good reasons for not wanting to enclose the vertex detector within the machine vacuum, the first material encountered by particles, which degrades the measurement of their impact parameters, is the beam-pipe. For the SLD upgrade detector, a beam-pipe of thickness 0.75 mm was used. This had a large safety factor with respect to the atmospheric pressure. The main risk was cracking during installation on the beam-line. For the TESLA detector, it is proposed to stabilise the delicate inner section of beam-pipe by means of a rigid clamp at $Z = \pm 15$ cm in the form of the two halves of the VTX support structure, as shown in Figure 6. This sturdy beryllium

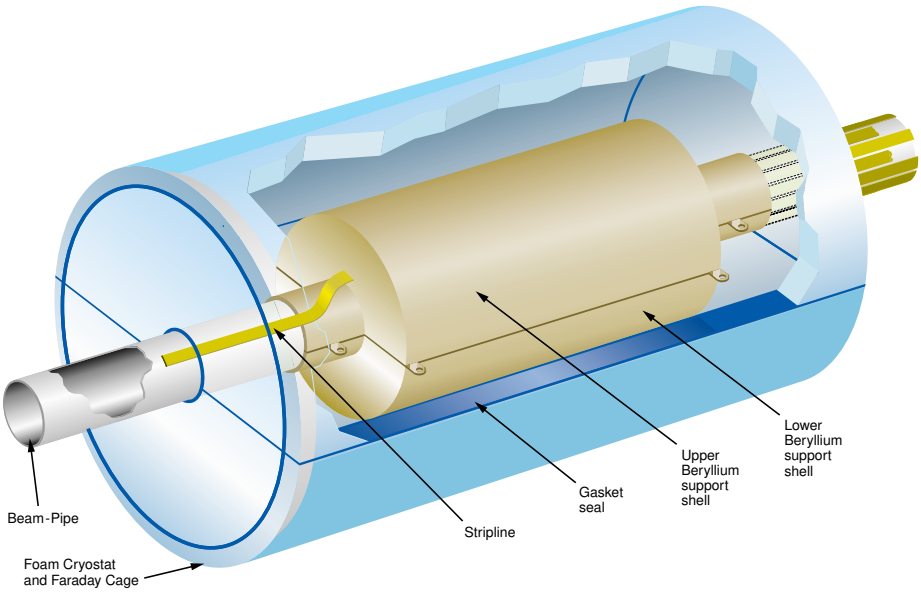

Figure 6: Isometric view of the detector, showing the support shell linking the robust outer sections of beam-pipe.

shell can be made with 1.5-2 mm wall thickness ($\leq$ 0.6% X_0) with no degradation to the tracking performance, since it lies beyond the system used to measure the impact parameter. By this method, it is considered possible to reduce the thickness of inner beam-pipe (a cylinder of length 12 cm) to 0.25 mm. However, this needs to be established with test structures, the main concern being stresses on the thick/thin braze joints during installation.

Given the approximately hermetic support shell, the gas cooling can be achieved by axial flow, feeding in at one endplate and out through holes in the other. The more robust cooling of the driver and readout chips can be achieved with evaporative cooling of nitrogen. While there is experience with these techniques in earlier detectors [7, 6] there are new aspects for the TESLA implementation which will require R&D. Minimising the external plumbing needed for the delivery and exhaust of the coolant requires some development; some improvements with respect to the rather satisfactory SLD system can be envisaged.

The construction principles of the 64-ladder detector have been described in Section 6. As with SLD, the detector would be surveyed optically during assembly, layer by layer. Unlike in SLD, due to the opaque support shell, the order of survey would be reversed, starting with layer-5, and would be carried out on each half-detector separately. As usual, the fine tuning of the geometry would be done by track fitting. Achieving systematic errors on a system of length 250,000 microns and diameter 120,000 microns which does not add significantly to the intrinsic precision of ~ 3 microns will be even more challenging than with the somewhat smaller (length 16 cm) SLD detector. The principle of construction based on ladder/annulus blocks fixed at one end and sliding at the other is a proven method of allowing for the otherwise massive effects of differential contraction between the ladders (all at slightly different temperatures) and the support shell (which will be slightly cooler at the bottom than the top). However, a new feature of the design concept is the stretched silicon. This has non-trivial consequences all the way through the construction from the stage of wafer thinning, mechanical assembly of ladders, attachment of driver and readout ICs, ladder testing, assembly into barrels and optical survey. The R&D programme to establish this design concept is well underway, with the first 2-CCD mechanical models (using unprocessed silicon of thickness 60 μm) having been successfully assembled as seen in Figure 7. This structure has been subjected to a rather extreme test in which the spring tension at the sliding end was repeatedly removed (so the ladder sagged visibly) and re-applied. Measuring the stability of sagitta 100 times, it was found (Figure 8) that for a spring tension in excess of 150 gms, the stability of sagitta was better than 3 μm. This is an excellent beginning, but the work has to be extended to cover the more realistic scenario of excursions around the nominal operating temperature of ~ 180 K (are there any serious stiction effects?) and assembly of silicon from processed CCD wafers, rather than the more uniform unprocessed material used for the initial studies.

8.2 Column-parallel CCDs

A column-parallel CCD is conceptually simpler than the 'standard' imaging device. Eliminating the readout register avoids many of the most complex aspects of the usual design. However, the requirement of being able to clock the parallel register at up to 50 MHz (for the layer-1 CCDs) is challenging. The most obvious need is to reduce the resistance of the buslines that run along the edge, and of the gates that distribute the clock pulses to the interior of the device area.

The key to solving both these problems lies in the fact that CCDs for particle detection are allowed to be opaque to visible light, which opens the possibility of providing wide aluminium buslines (say 0.3 mm wide) deposited mostly on top of the polyimide passivation layer, overlapping the imaging area but also contacting the 'standard' aluminium buslines deposited on the silicon dioxide surface. This will provide much reduced busline resistance with no serious increase in capacitance.

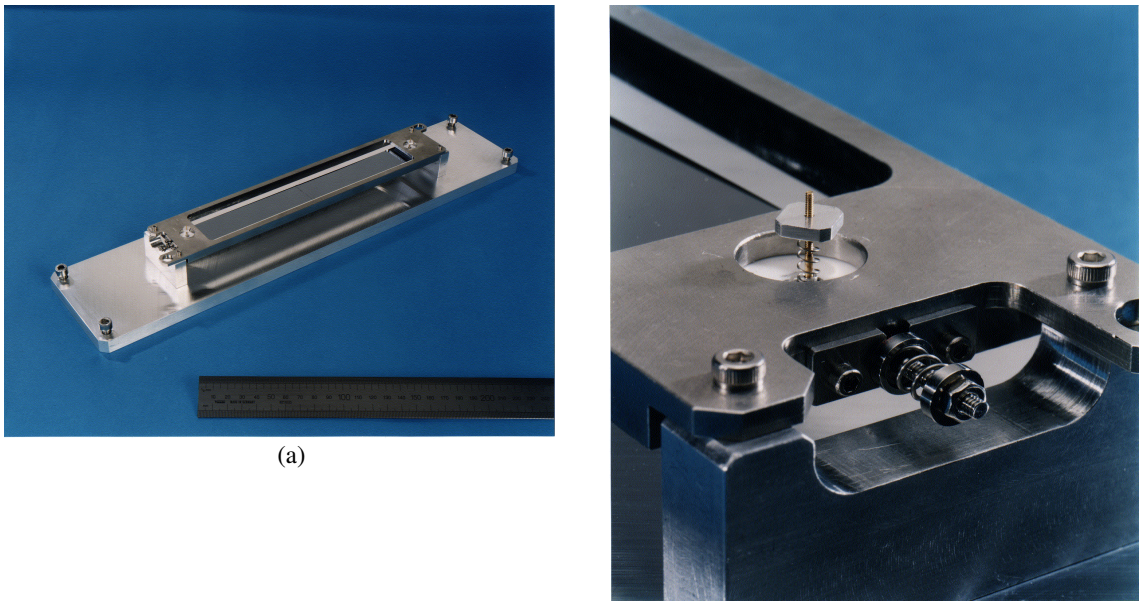

(a) (b)

Figure 7: (a) Photograph of mechanical prototype of a 2-CCD silicon ladder of thickness 60 μm , with (b) details of the spring tensioning system at one end.

Similarly, it will be possible to overlay the polysilicon gates in the imaging area with aluminium strips to reduce their resistance. These features are of course not sufficient. One needs also to carefully control the inductances, on-CCD and in the connections from the local driver IC. It is clear that the most promising CCD architecture will be 2-phase with sinusoidal drive waveforms, since this preserves a perfect balance between the currents flowing in the two phases, minimising clock feedthrough to the sensitive output circuits. Various options have been studied in P-SPICE simulations. One example in which realistic wire-bond inductances have been included between the driver and CCD is shown in Figure 9, indicating that drive pulses of excellent fidelity should be achievable over the entire surface area of the layer-1 CCDs. CCDs on the outer layers are each connected electrically at only one end, but the required clocking rates are lower. The power dissipation associated with clocking the overall detector at 'standard' CCD voltages would be excessive, but can be drastically reduced due to two fortunate circumstances. Firstly, the potential wells needed to transfer the small charge packets (signal and background) can be relatively shallow. By careful control of the implants for 2-phase clocking, it is expected that drive pulse amplitudes in the range 1-3 V will prove sufficient, as already developed for some CCDs in lightweight video cameras. Secondly, the CCD clocking, as well as all the dissipative electronics, needs to be operated only during the bunch train (with a short early settling period), giving only ~ 0.5% duty cycle. Following these procedures, the average power dissipation in the active volume of the detector with 799 Mpixels is calculated to be less than 10 W, easily cooled by a gentle flow of nitrogen gas, as used at SLD.

The readout system for the column parallel CCDs will be the subject of an intense R&D programme. The general scheme consists of minimal on-CCD processing, with bump-bond connections to the readout chip, where advantage can be taken of the very small scale integrated electronics possible with CMOS using feature sizes of 0.25 μm or below (probably approaching 0.1 μm during the lifetime of the project). Already the CCD design team at Marconi has been able to lay out 2-stage source follower circuits with constant-current first-stage load transistors, on a pitch of 20 μm , as shown in Figure 10. While the second-stage currents in this initial design would be excessive, it appears that the external load to be driven (bump-bond connection and preamp input) will be sufficiently small to permit 50 MHz operation with only a single stage source follower on the CCD.

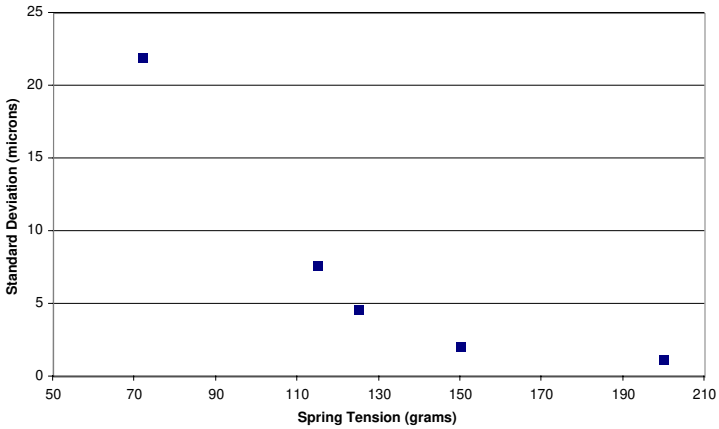

Figure 8: Sagitta stability as function of tension applied to the unsupported silicon.

Again, pulsed power will be used to keep the dissipation under control. Furthermore, this circuitry is beyond the edge of the active volume, so more robust cooling systems are acceptable, as discussed in Section 6.

There are various subtle features of the CCD operation, such as the need for fast charge collection into the buried channel, so the epitaxial region will be fully depleted, and the clock phases synchronised accurately with bunch crossings. The Lorentz angle effects from the 4T solenoid field are significant. For these and other reasons, accurate 3-D simulation of the devices under dynamic operating conditions will be essential. These will be carried out at two of the collaborating institutes, where the necessary software tools are currently available.

The row of bump-bonds connecting the CCD to the readout chip (Figure 11) will be staggered to give a minimal pitch of ~ 40 μm , which complies with easily available industrial standards.

8.3 Readout IC

Thinking about the design of the readout chip is only beginning, but it rests on firm foundations, notably the edge logic already developed for CMOS imaging devices [9]. There are a number of options for the front-end, but one which will at least come close to optimising the noise performance will be a single-stage source follower on the CCD with only occasional reset (possibly only between bunch trains), AC coupled with < 1 μs time constant to the preamp input on the readout chip, of which the general functionality is indicated in Figure 12. 4-6 bit ADCs operating at 50 MHz can be accommodated within the 20 μm pitch. The next step comprises digital subtractions between successive pixel signals, sensing the signal steps while discarding the empty data on the trailing edge of real signals. These subtracted pixel data are subjected to a pixel threshold set at approximately twice the standard deviation of the readout noise, low enough for full min-I efficiency but too low to be used as the sole means of data sparisification. Signals which satisfy the pixel threshold are used to activate kernel logic which checks the overall signal in any 2×2 cluster around the trigger pixel. All pixel signals from clusters which satisfy the cluster threshold are stored in local memory. Sparse data clusters are assembled in a particular format (address, followed by pixel contents in a standard order) and stored in memory which will probably consist of a separate chip mounted on the ladder block adjacent to the readout chip.

8.4 Driver IC

Design of the driver IC is expected to follow the technology used for mobile phone and other small-scale RF applications. Discussions are just beginning with experts in this field.

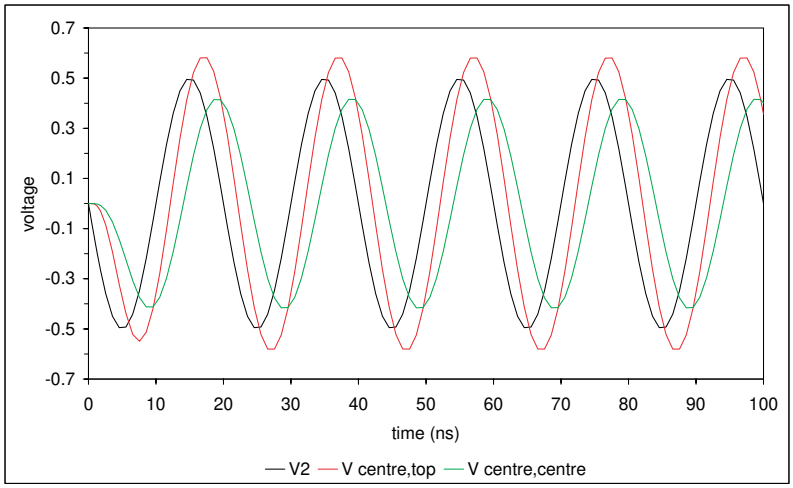

Figure 9: 1 phase of 2-phase clock waveforms at extreme positions of the CCD imaging area, for a layer-1 CCD operated at 50 MHz.

8.5 Radiation damage effects

Due to the faster clocking and hence more frequent filling of traps, the TESLA detector will be less susceptible to bulk damage than at SLD, where excellent performance was achieved. However, there are still some concerns about neutron damage, which could be serious only if flux levels greatly exceed current expectations. The readout chip could be susceptible to single-event upsets (SEUs) or long-term damage. In any case, the radiation tolerance of modern CCDs with respect to neutrons, over a wide range of operating temperatures, is not well characterised. One of the essential goals of the LCFI collaboration is to provide a comprehensive study of the radiation effects in the CCDs and readout chips with different device architectures (supplementary channels etc) as a function of temperature. Much of the infrastructure to carry out these important studies is now in place.

9 Outlook

As a result of a large amount of imaginative design and hard work, the TESLA accelerator scientists have been able to deliver a beam-pipe radius of 14 mm at the IP, which presents an excellent opportunity for heavy flavour physics. The detector physicists have responded by sketching various pixel-based designs which (if realised) will provide all the tools needed for vertex detection in the TeV regime. What is now needed is an intensive period of R&D in order to see which of these ideas can be turned into reality.

For the CCD option, the thinking has been based on the SLD experience. However, the first SLD vertex detector required 6 years of R&D, and the challenges for the future LC (TESLA or NLC) are at least as great. The LCFI collaboration was funded for a startup R&D programme in 1998. Progress over the past two years has made it possible to define the overall requirements in order to demonstrate the feasibility of the detector concept, with a few working ladders. With good luck, this could be achieved over the next 4 years. However there are bound to be setbacks, and a 6-year R&D period (as for SLD) would appear to be more realistic.

Other pixel-based options for the TESLA vertex detector are of course being pursued in parallel by other groups, notably CMOS pixels and hybrid pixel systems. As well as this healthy and important competition, the boundary conditions will only be clearly defined when the world community decides which LC option to build. Even if TESLA were not selected, the vertex detector development work now underway for the CCD and other pixel-based options is generic. Apart from details of the

readout IC, the designs under development could be applied equally to all the LC accelerator and detector systems being considered today. It is probably a mistake to expect one technology for TESLA to prove 'the winner', and an even bigger mistake to predict which that will be. There are many unknown factors. Furthermore, due to some glitch in the R&D programme, the potentially highest performance option could be delayed. In this case, the second-choice option could be implemented for the first phase of the physics programme. For this and other reasons, the need for access to the inner detector region of TESLA has been given high priority, in the overall detector design.

Details of the CCD detector design, such as fine tuning of the pixel dimensions for optimal precision while respecting the constraints of 2-track resolution, will be based on future simulation of physics processes of interest.

While the R&D programme outline in Section 8 is focused on the requirements for a vertex detector at the future LC, it is clear from discussions with CCD designers and colleagues in astronomy and SR detection, that the systems being developed will be of great interest to other areas of science and technology. The factor 100-1000 speed increase in CCD readout will be useful to several fields in which time resolved images with visible light or X-rays at high frame-rate are desired. Imaging devices are so pervasive in their applications that technical developments in one area can be guaranteed to spill over into other areas. Without explicitly engaging in inter-disciplinary programmes, the communication channels provided by the scientists who design the CCDs for scientific applications have a long and impressive track record for feeding ideas between their numerous application areas. These informal communication channels have over many years been far more effective than 'specially promoted programmes' and other short-term initiatives from governments and scientific funding agencies.

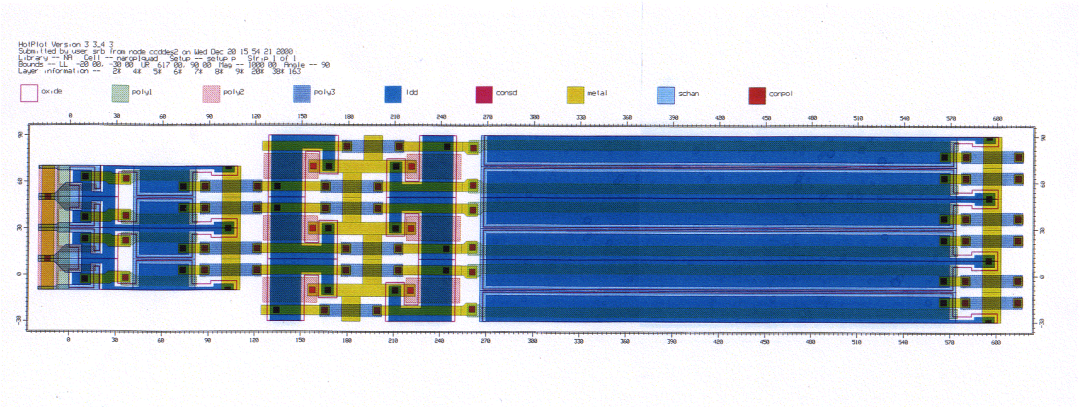

Figure 10: Provisional layout of CCD output circuits on pitch of 20 μm .First-stage source followers on left, second-stage on right.

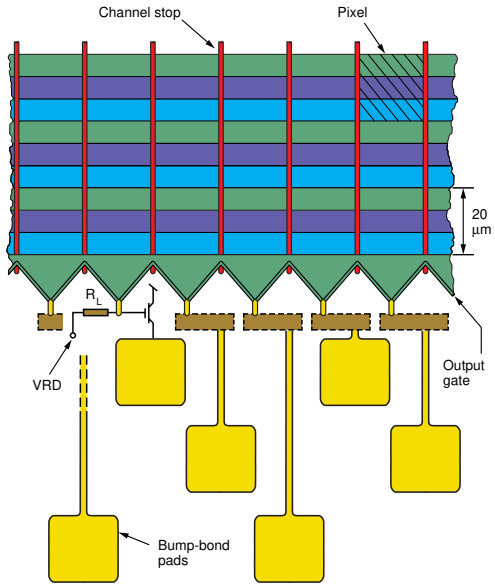

Figure 11: Edge of column parallel CCD in region of interface to readout chips.

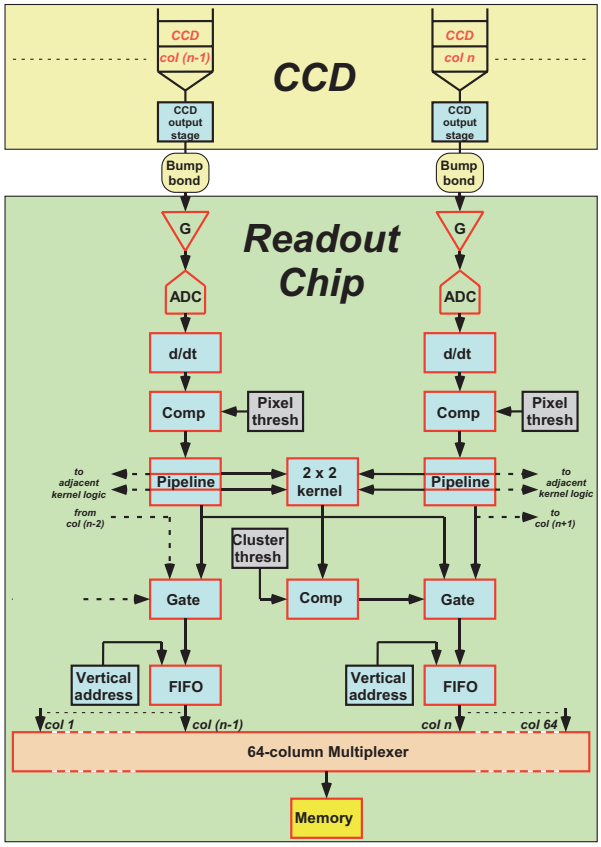

Figure 12: Logic layout of readout integrated circuit.

References

[1] DJ Jackson, *Nucl Instr Meth* **A388** (1997)247

[2] S Xella Hansen et al, LC-PHSM-2001-024 (DESY LC note)

[3] LCFI Collaboration web page http://hep.ph.liv.ac.uk/~green/lcfi/home.html

[4] CK Bowdery and CJS Damerell, Workshop on Physics and Experiments with Linear Colliders, Waikoloa, Hawaii, World Scientific (1993) 773

[5] GD Agnew et al, Proc 26th International Conference on High Energy Physics, Vol 2 p1862, Dallas, 1992, World Scientific, New York 1992

[6] K Abe et al, *Nucl Instr Meth* **A400** (1997) 287

[7] CJS Damerell, Proc Physics in Collision IV, 1984 (Editions Frontieres) (1985) 453

[8] R Hawkings, LC-PHSM-2000-021 (DESY LC note)

[9] ER Fossum, *IEEE Trans Electron Devices*, **44** (1997) 1689